PROCEEDINGS OF SCIENCE

Simulation of In-ice Askaryan Radiation from Air Shower Cores for Cosmic Rays Search with RNO-G

The RNO-G Collaboration

(a complete list of authors can be found at the end of the proceedings)

E-mail: noppadol@udel.edu, agnlesz@udel.edu, dseckel@udel.edu

The Radio Neutrino Observatory in Greenland (RNO-G) was designed to detect ultra-high energy neutrinos through Askaryan radiation. The detector utilizes radio antennas that are deployed both just below the ice surface and inside the ice boreholes to observe radio signals that come from above and below the ice surface. However, high energy cosmic rays' in-ice cores also produce radio emission and are expected to be observed with in-ice antennas. The recently developed Framework for the simulation of Air shower Emission of Radio for In-ice Experiments, FAERIE, allows us to simulate radio pulses present at in-ice antennas with high precision but at great computational cost. Given the large variations in energy and development of air shower cascades, the ability to quickly and efficiently simulate radio emission from air showers as seen by the in-ice antennas becomes imperative. In this study, we present an efficient simulation method that reduces computing time but maintains significant features of the Askaryan radio signals such as timing, polarization, and overall amplitude footprint. This enables various studies that require a large volume of simulations like classification of cosmic ray candidates, training neural networks, and events reconstruction.

Corresponding authors: Noppadol Punsuebsay[1*], Agnieszka Leszczynska[1], David Seckel[1]

[1] *Bartol Research Institute and University of Delaware*

[*] Presenter

39th International Cosmic Ray Conference (ICRC2025)
15–24 July 2025
Geneva, Switzerland

ICRC 2025
The Astroparticle Physics Conference
Geneva July 15-24, 2025

PoS(ICRC2025)366

1. Introduction

The primary goal of Radio Neutrino Observatory in Greenland (RNO-G) located at the Summit station is to detect ultra-high-energy neutrinos using radio antennas placed just underneath ice surface and inside boreholes up to ~100 meters deep [1, 2]. When neutrinos interact with Greenland ice, they generate cascades of secondary particles that emit a coherent radio signal called Askaryan radiation that arises from the charge imbalance in the cascades [3].

Cosmic-ray (CR) air showers also produce radio emissions, making it challenging to distinguish them from neutrino events without simulations [4]. Secondary particles from air showers that reach the ice surface can further produce more cascades in the ice called the *shower core*. The electric field contribution from a particle shower in the atmosphere is called *in-air emission* and that from the shower core in the ice is called *in-ice emission*. The cascades of shower core generate negative charge excess similar to in-ice neutrino-induced showers, but with a different shower geometry. The FAERIE framework models electric fields at in-ice antennas, calculating in-air emissions using CoREAS and CORSIKA7 [5] and in-ice emissions using a module based on GEANT4 toolkit [6].

With FAERIE's default settings, simulating in-ice emissions from an air shower initiated by a proton at 100 PeV and 0° zenith angle took ~3000 CPU hours for 121 antennas [7]. This study aims to optimize FAERIE's runtime on computing in-ice emission while maintaining output quality for large-scale simulations, especially within the RNO-G collaboration for deep CR search [8, 9].

2. Scope and Strategy

There are three main steps in FAERIE. The first step is running the in-air shower simulation with CORSIKA and CoREAS. FAERIE uses CORSIKA with modified version of CoREAS allowing it to propagate in-air emission to antennas below the ice surface [7]. Then, it extracts the CORSIKA ground-level particles to generate input files for the GEANT4-based module. The last step is running the in-ice shower simulation with the GEANT4-based module [10].

The particle output files contain the list of ground-level particles with their identification number, momentum, position, time, and weight inherited from CORSIKA thinning. Total runtime for in-ice simulation consists of the module setup time, cascade calculation and the calculation of emission to the antennas. Setup time scales with number of antennas, cascade calculation scales with total simulated particle energy, and radio emission scales with both. Our goal is to reduce the computational load without modifying the GEANT4-based module's internal code, so we focus on only altering particle properties during file processing and adding detector simulation at the end to obtain simulations that are comparable to data.

3. FAERIE Modification

This section will focus mainly on different modification methods (**modes**). We used a vertical proton-induced air shower at 1 PeV with 225 antennas (reference shower S_1). The particles in the shower are sorted into two-dimensional bins defined by discrete energy intervals and radius intervals (lateral distance from the shower axis) to determine the appropriate approach. We can see the shower structure in figure 1 lower energy particles are at a greater distance from the shower axis,

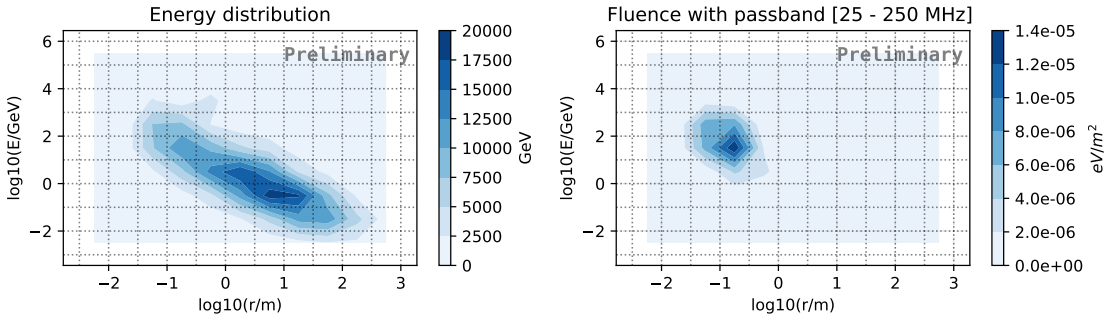

Figure 1: Contour maps show total particle energy (**left**) and integrated power of electric field (**right**) contributed by ground-level photons within each radial-energy bin.

while the highly energetic particles traverse closer to the axis and emit a stronger coherent signal. We explore the effects of adding energy cut, particle filtering, and energy modification iteratively in each consecutive mode.

3.1 Mode 1

Mode 1 is the default operation of FAERIE. FAERIE discards particles outside 1 m from the shower axis and divides the list into energy bins and then into parts [7]. The total CPU time spent computing in-ice emission from the reference shower S_1 was ~ 80 hr.

3.2 Mode 2

As discussed above, high-energy photons in air showers are closer to the core while lower-energy photons spread out and are less coherent. Based on figure 1 we apply an energy cut at $E_{cut} = 10$ GeV in mode 2, reducing the computational effort while preserving the coherent signal.

3.3 Mode 3

Because in-ice emission arises from a charge imbalance in electromagnetic (EM) cascade producing coherent radiation, in mode 3, we only keep EM particles (γ, e^+, e^-) along with energy and radius cuts from the prior modes. The electric field amplitude difference between mode 1 and

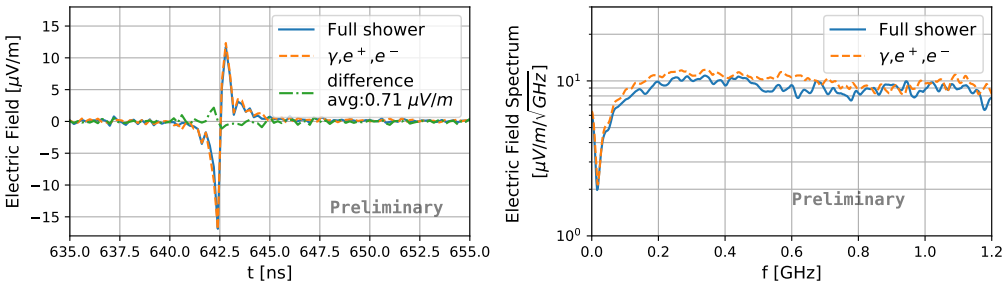

Figure 2: Vertical component of simulated electric fields using full particle list (solid) and EM particles (dashed) in time domain and frequency domain at a selected antenna. Difference between using the two particle selection is shown by dashed green line.

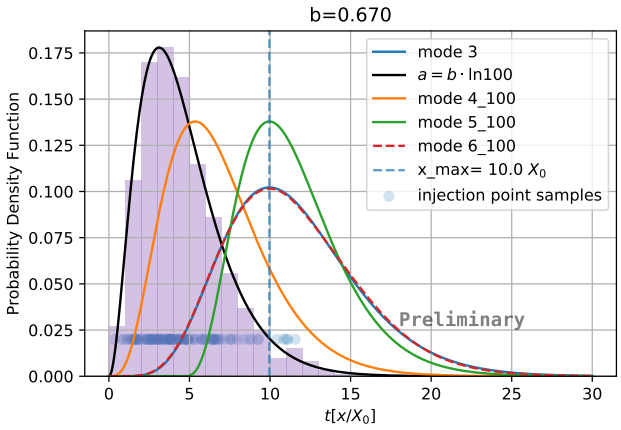

Figure 3: Expected average shower profiles of 1 TeV photon after being modified with mode 3 and 4-6 with $\beta = 100$. Injection distribution follows $\Gamma(a, b)$ where $a = b \ln(\beta)$.

3 is shown to be $\sim$ 10% in figure 2. The total CPU time for computing in-ice emission of our reference shower S_1 was $\sim$ 60 hr in this mode.

Mode 2-3 extend basic filtering for energy cut and particle identification, reducing electric field calculation time by $\sim$ 25% vs standard FAERIE. In mode 4-6, we lower each particle's energy to reduce runtime, adjust weight to compensate for signal strength, and modify particle injection to preserve the shower profile.

3.4 Mode 4

Let β be a computation reduction factor. In this mode, for each particle in the output file, we scale its energy E and weight w, derived from CORSIKA thinning, to be $E' = E/\beta$ and weight $w' = \beta \cdot w$. The total CPU time for simulating the reference shower S_1 was $\sim$6 hr when $\beta = 10$. To study effects of modification of energy on pulse shape and time, we use simulations of single high-energy photon injected in the ice instead of ground-level particles from an air shower. In this case, mode 3 was equivalent to mode 1 and mode 4 yielded shorter longitudinal profile and shallower shower maximum due to being simulated at lower energy.

3.5 Mode 5

An electromagnetic shower's maximum X_{max} (in radiation length units) is related to the initial particle's energy E and critical energy E_c by $X_{max} \approx \ln(E/E_c)$ [11]. As a result, $X_{max} - X'_{max} \approx \ln(\beta)$. In mode 5, we correct shower maximum by displacing particles along their momentum directions $\hat{p}$ such at line integral of ice density profile equals to $X_0 \ln(\beta)$ where X_0 is the radiation length. In this mode, the shower profile becomes narrower as β increases, which motivates for mode 6.

3.6 Mode 6

The shower profile follows gamma distribution with shape parameter a and rate parameter b, where $X_{max} = (a-1)/b$. A property of gamma distribution states that if $X \sim \Gamma(a_x, b)$ and $Y \sim \Gamma(a_y, b)$ are both random and independent variables, $X + Y \sim \Gamma(a_x + a_y, b)$ [12]. Generally,

the b value depends on material and energy, but we assume that b is constant. If we randomly sample positions from the distribution X to inject particles with profile Y, resulting profile is $X+Y$. With property of gamma distribution and relationship between a, b, X_{max}, we conclude that $a_{injection} = a - a' = b(X_{max} - X'_{max}) = b\ln(\beta)$. Injection positions are calculated in radiation length units and account for particle momentum and ice density profile. In figure 3, we represent expected profiles from 1 TeV photon modified with different modes, and mode 6 injection profile.

3.7 Thinning

Mode 6 allows us to use larger β, but this causes the lower-energy particles to be at energies lower than the critical energy after modification. To avoid this behavior and maintain the target computation reduction factor β, a particle i with energy E_i that satisfies thinning condition $E_i/\beta < E_{thin}$ would be added to thinning batch $\{E_i\}$. An energy lower bound $E_{threshold}$ was set to ensure minimum energy implying maximum energy scaling factor allowed to be $\beta_{max} = E_{cut}/E_{threshold}$. Then thinning probability q would be $q = \beta_{max}/\beta$. In the case of $\beta = 1000$, $E_{cut} = 10$ GeV, and $E_{thin} = E_{threshold} = 0.1$ GeV, particles at 10-100 GeV will be thinned with thinning probability $q = 0.1$

4. Modification Performance

We initiated a 1 TeV photon at the ice surface, modified the particle with mode 3-6, and then simulated it 100 times. Average shower profile reflects our expectation of each mode. We fit theoretical curves to normalized averages from figure 4 and show the comparison in figure 5, in which they are indeed in good agreement. We apply fitted $b = 0.67$ to mode 6 implementation.

Next, we simulate a 10 PeV vertical, proton-initiated air shower with 225 antennas (reference shower S_2) for performance testing. In addition to FAERIE modules, we folded electric field output with RNO-G antenna and electronics response without noise using another Python submodule from

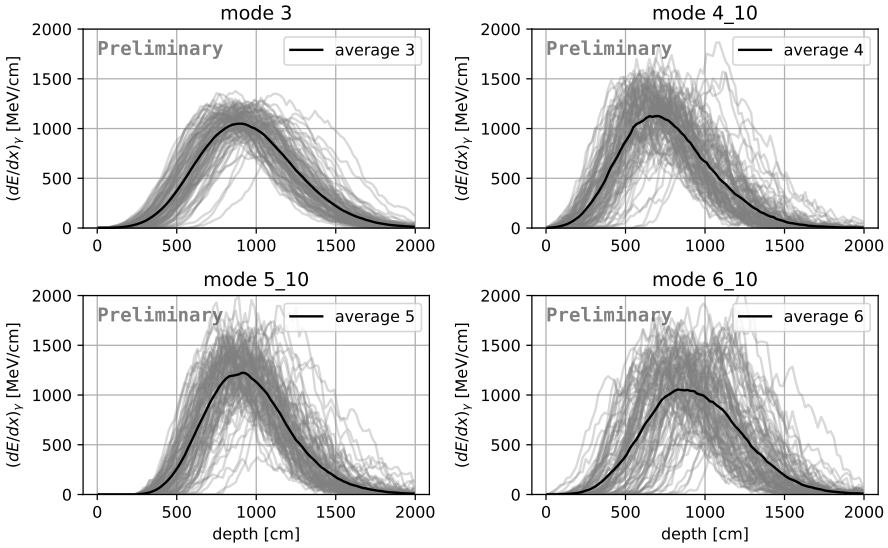

Figure 4: Longitudinal energy profiles of single 1 TeV photons simulated 100 times for each different modes.

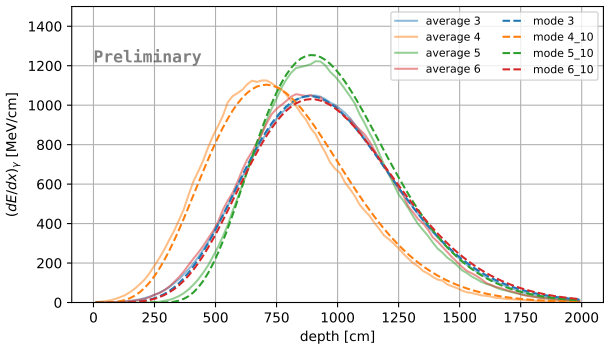

Figure 5: Average energy deposition profiles from different modes with their theoretical expectations, using $b = 0.67$ and scaled such that total energy deposited or area under the curves were equal to their corresponding profile.

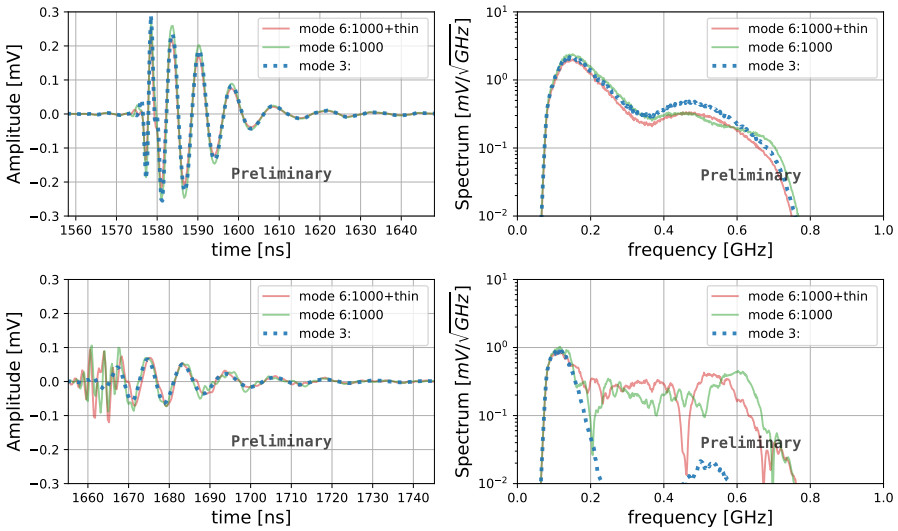

Figure 6: Panels showed example waveforms in time domain (**left**) and frequency spectrum (**right**) from an on-ring antenna (**top**) and an off-ring antenna (**bottom**).

a *NuRadioReco* framework [13]. The quality of simulated voltage trace depends on its antenna location relative to the Cherenkov ring, which is a ring-like pattern of coherent signal generated near Cherenkov angle. Figure 6 shows example waveforms from on-ring and off-ring antennas while figure 7 shows amplitude and pulse time errors on a rectangular grid. We use the Hilbert envelope peak and its time to represent pulse amplitude and arrival time at an antenna. The standard deviation of the amplitude difference is $\sim$ 12% and that of pulse time is $\sim$ 2 ns. The total runtime for shower S_2 was ~80 min for mode 6 with $\beta = 1000$ and thinning, as compared to an estimated 600 hrs for mode 3.

5. Summary and Outlook

We presented simple methods that filter and modify input particles and their properties instead of changing the field calculation directly. We have shown that computational load reduction factor β can be as high as 1000 with mode 6 and thinning at 10 PeV. Total CPU time spent simulating

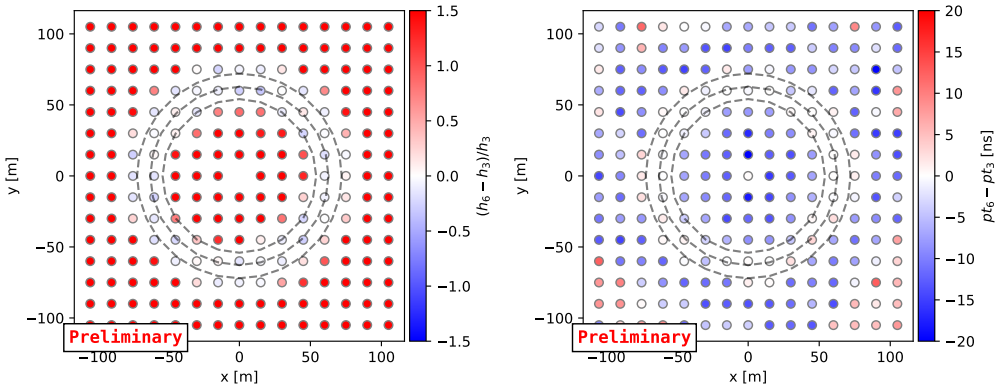

Figure 7: Grid pattern of Hilbert peak h and pulse time pt discrepancies between mode 3 and mode 6 with $\beta = 1000$ and thinning on 15×15 rectangular grid. A band spanning the radiation launching angle range of $\theta_c \pm 5°$,illustrated by red dashed lines, marks the region where strong coherent signals are anticipated.

100 PeV vertical proton-induced shower with 100 antennas is $\sim$ 5 hr comparing to $\sim$ 3000 hr with 121 antennas prior to modification. As described in section 2, total runtime consists of setup time, cascade calculation, and propagating electric fields to the 100 antennas which took approximately 1, 0.5, and 3.5 hr, respectively. Similar studies were done at different zenith angles, and we see appropriate effects of polarization and shower geometry, but results are not presented here.

While execution time diminished significantly with increasing β, amplitude and pulse time errors arose due to additional high-frequency content, especially in the region off the Cherenkov ring. This may be explained by the modified injection, thinning and reweighting procedure. Although our procedure preserves the expected longitudinal deposited energy shower profile, shorter subshowers produce lumpier realizations. The radiation from these lumps will be in phase for antennas near the Cerenkov ring, so these signals are preserved; but for offset antennas, the lumpier subshowers experience less *destructive* interference, especially at higher frequencies. If correct, the high frequency excess would be reduced for higher energy showers, with a finer grained distribution of subshowers. This will be studied in future work.

Originally, FAERIE specifies maximum number of particles in each file to limit maximum job runtime in parallel computing. Due to mode 6, the simulated energy is reduced by factor β resulting in fewer files and reducing overhead cost but maintaining maximum job runtime with fewer number of jobs. Please note that the discussion of execution time in the above sections does not include CORSIKA simulation due to its long simulation time. The above results (Fig 1, 2) show that

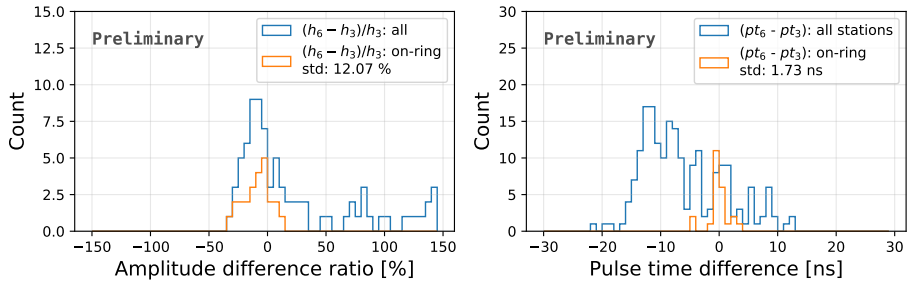

Figure 8: Histogram depicted distribution of relative amplitude (**left**) and pulse time (**right**) from all antennas (**blue**) and on-ring antennas (**orange**).

E_{cut} = 10 GeV does not significantly impact the in-ice emission. We changed CORSIKA's ECUT to 3 GeV so that the in-air simulation time also reduced significantly, but expect such a change would require a modification to how FAERIE treats in-air emission. Optimization of runtime that depends of number of antenna and job files would be discussed in the future study. Achieving this level of efficiency turns simulation tasks that would have taken years of CPU time to hours. This framework can enable accurate modeling of CR pulses that could be used as templates in a CR search, determining expected rates, identifying backgrounds, and validating the concept of in-ice radio measurement [8, 9].

References

[1] **RNO-G** Collaboration, A. Nelles *et al. PoS* **ICRC** no. 1129, (2025) .

[2] **RNO-G** Collaboration, S. Agarwal *et al. JINST* **20** no. 04, (2025) P04015.

[3] G. A. Askar'yan *Soviet Journal of Experimental and Theoretical Physics* **21** (Sept., 1965) 658.

[4] S. W. Barwick and C. Glaser *Encyclopedia of Cosmology II* (2023) 237–302.

[5] D. Heck, J. Knapp, J. N. Capdevielle, G. Schatz, and T. Thouw, *CORSIKA: a Monte Carlo code to simulate extensive air showers.* 1998.

[6] S. De Kockere, K. D. de Vries, N. van Eijndhoven, and U. A. Latif *Phys. Rev. D* **106** (Aug, 2022) 043023.

[7] S. De Kockere, D. Van den Broeck, U. A. Latif, K. D. de Vries, N. van Eijndhoven, T. Huege, and S. Buitink *Phys. Rev. D* **110** (Jul, 2024) 023010.

[8] **RNO-G** Collaboration, B. Hendricks *et al. PoS* **ICRC** no. 1057, (2025) .

[9] **RNO-G** Collaboration, M. Liu *et al. PoS* **ICRC** no. 319, (2025) .

[10] S. De Kockere, "Iceshelf." `https://github.com/sdekockere/IceShelf/tree/main`, 2013.

[11] **Particle Data Group** Collaboration, S. Navas *et al. Phys. Rev. D* **110** no. 3, (2024) 030001.

[12] R. V. Hogg and A. T. Craig, *Introduction to mathematical statistics*. Macmillan, London, England, 4 ed., Mar., 1978.

[13] C. Glaser, A. Nelles, I. Plaisier, C. Welling, S. W. Barwick, D. García-Fernández, G. Gaswint, R. Lahmann, and C. Persichilli *European Physical Journal C* **79** no. 6, (June, 2019) 464.

PoS(ICRC2025)366

Full Author List: RNO-G (June 30th, 2025)

S. Agarwal[1], J. A. Aguilar[2], N. Alden[3], S. Ali[1], P. Allison[4], M. Betts[5], D. Besson[1], A. Bishop[6], O. Botner[7], S. Bouma[8], S. Buitink[9,10], R. Camphyn[2], J. Chan[6], S. Chiche[2], B. A. Clark[11], A. Coleman[7], K. Couberly[1], S. de Kockere[12], K. D. de Vries[12], C. Deaconu[3], P. Giri[13], C. Glaser[7], T. Glüsenkamp[7], H. Gui[4], A. Hallgren[7], S. Hallmann[14,8], J. C. Hanson[15], K. Helbing[16], B. Hendricks[5], J. Henrichs[14,8], N. Heyer[7], C. Hornhuber[1], E. Huesca Santiago[14], K. Hughes[4], A. Jaitly[14,8], T. Karg[14], A. Karle[6], J. L. Kelley[6], C. Kopper[8], M. Korntheuer[2,12], M. Kowalski[14,17], I. Kravchenko[13], R. Krebs[5], M. Kugelmeier[6], R. Lahmann[8], C.-H. Liu[13], M. J. Marsee[18], K. Mulrey[10], M. Muzio[6,5], A. Nelles[14,8], A. Novikov[19], A. Nozdrina[4], E. Oberla[3], B. Oeyen[20], N. Punsuebsay[19], L. Pyras[14,21], M. Ravn[7], A. Rifaie[16], D. Ryckbosch[20], F. Schlüter[2], O. Scholten[12,22], D. Seckel[19], M. F. H. Seikh[1], Z. S. Selcuk[14,8], J. Stachurska[20], J. Stoffels[12], S. Toscano[2], D. Tosi[6], J. Tutt[5], D. J. Van Den Broeck[12,9], N. van Eijndhoven[12], A. G. Vieregg[3], A. Vijai[11], C. Welling[3], D. R. Williams[18], P. Windischhofer[3], S. Wissel[5], R. Young[1], A. Zink[8]

[1] University of Kansas, Dept. of Physics and Astronomy, Lawrence, KS 66045, USA
[2] Université Libre de Bruxelles, Science Faculty CP230, B-1050 Brussels, Belgium
[3] Dept. of Physics, Dept. of Astronomy & Astrophysics, Enrico Fermi Inst., Kavli Inst. for Cosmological Physics, University of Chicago, Chicago, IL 60637, USA
[4] Dept. of Physics, Center for Cosmology and AstroParticle Physics, Ohio State University, Columbus, OH 43210, USA
[5] Dept. of Physics, Dept. of Astronomy & Astrophysics, Center for Multimessenger Astrophysics, Institute of Gravitation and the Cosmos, Pennsylvania State University, University Park, PA 16802, USA
[6] Wisconsin IceCube Particle Astrophysics Center (WIPAC) and Dept. of Physics, University of Wisconsin-Madison, Madison, WI 53703, USA
[7] Uppsala University, Dept. of Physics and Astronomy, Uppsala, SE-752 37, Sweden
[8] Erlangen Centre for Astroparticle Physics (ECAP), Friedrich-Alexander-University Erlangen-Nürnberg, 91058 Erlangen, Germany
[9] Vrije Universiteit Brussel, Astrophysical Institute, Pleinlaan 2, 1050 Brussels, Belgium
[10] Dept. of Astrophysics/IMAPP, Radboud University, PO Box 9010, 6500 GL, The Netherlands
[11] Department of Physics, University of Maryland, College Park, MD 20742, USA
[12] Vrije Universiteit Brussel, Dienst ELEM, B-1050 Brussels, Belgium
[13] Dept. of Physics and Astronomy, Univ. of Nebraska-Lincoln, NE, 68588, USA
[14] Deutsches Elektronen-Synchrotron DESY, Platanenallee 6, 15738 Zeuthen, Germany
[15] Whittier College, Whittier, CA 90602, USA
[16] Dept. of Physics, University of Wuppertal D-42119 Wuppertal, Germany
[17] Institut für Physik, Humboldt-Universität zu Berlin, 12489 Berlin, Germany
[18] Dept. of Physics and Astronomy, University of Alabama, Tuscaloosa, AL 35487, USA
[19] Dept. of Physics and Astronomy, University of Delaware, Newark, DE 19716, USA
[20] Ghent University, Dept. of Physics and Astronomy, B-9000 Gent, Belgium
[21] Department of Physics and Astronomy, University of Utah, Salt Lake City, UT 84112, USA
[22] Kapteyn Institute, University of Groningen, PO Box 800, 9700 AV, The Netherlands

Acknowledgments

We are thankful to the support staff at Summit Station for making RNO-G possible. We also acknowledge our colleagues from the British Antarctic Survey for building and operating the BigRAID drill for our project.

We would like to acknowledge our home institutions and funding agencies for supporting the RNO-G work; in particular the Belgian Funds for Scientific Research (FRS-FNRS and FWO) and the FWO programme for International Research Infrastructure (IRI), the National Science Foundation (NSF Award IDs 2112352, 2111232, 2111410, 2411590, and collaborative awards 2310122 through 2310129), and the IceCube EPSCoR Initiative (Award ID 2019597), the Helmholtz Association, the Swedish Research Council (VR, Grant 2021-05449 and 2021-00158), the University of Chicago Research Computing Center, and the European Union under the European Unions Horizon 2020 research and innovation programme (grant agreements No 805486), as well as (ERC, Pro-RNO-G No 101115122 and NuRadioOpt No 101116890).